IEEE Access
Multidisciplinary | Rapid Review | Open Access Journal

Received 15 June 2022, accepted 19 July 2022, date of publication 25 July 2022, date of current version 11 August 2022.

Digital Object Identifier 10.1109/ACCESS.2022.3193769

RESEARCH ARTICLE

Classification of Current Density Vector Maps for Heart Failures Using a Transfer Convolutional Neural Network

ZHENGHUI HU, YUTONG LIN, KAIKAI YE, AND QIANG LIN
College of Science, Zhejiang University of Technology, Hangzhou 310023, China

Corresponding author: Zhenghui Hu (zhenghui@zjut.edu.cn)

This work was supported in part by the National Key Research and Development Program of China under Grant 2018YFA0701400, and in part by the Public Projects of Science Technology Department of Zhejiang Province under Grant LGF20H180015.

ABSTRACT Ischemic heart disease (IHD) is the leading cause of death worldwide. Magnetocardiogram (MCG) as a non-invasive detection of the heart, takes a more important role in clinic detection. However, the MCG technique is not a common diagnostic tool in routine clinical practice because of the lack of MCG data and trained doctors for MCG data, especially for current density vector map (CDVM). Therefore, we propose an automatic method to analyze MCG data using the deep learning method. Here, we propose a deep learning method called Residual Network (ResNet) with transfer learning to classify CDVM from category 0 to category 4, which is reconstructed from MCG data. The ResNet exhibited an accuracy of 90.02%. This paper suggests a high potential for applying ResNet to CDVMs.

INDEX TERMS Current density vector map (CDVM), magnetocardiogram (MCG), residual network (ResNet), transfer learning.

I. INTRODUCTION

Ischemic heart disease (IHD), also called coronary artery disease (CAD), is a disease with a high mortality rate in many countries [1], [2]. It can cause myocardial damage, resulting in myocardial infarction, ventricular arrhythmia, even sudden cardiac death and other severe consequences. IHD is preventable, early diagnosis and appropriate intervention are essential to reduce mortality [3]. Usually, when patients experience chest pain, it may be due to this disease.

As a diagnostic method, ECG accounts for a large part of routine clinical diagnosis. A 12-lead resting electrocardiogram (ECG) is frequently used. However, due to its lower sensitivity and specificity [4], in some cases, the ECG may not be significantly abnormal. For those patients with unexplained chest pain, invasive diagnostic methods may be unavoidable. For example, coronary angiography (CAG) is a safe and reliable invasive diagnostic technique, known as the gold standard for IHD diagnosis. However, invasive detection methods often have limitations, such as high cost of time and requiring technical experts to operate.

Also, as a non-invasive, contactless, radiation-free and risk-free multichannel mapping technology, magnetocardiogram (MCG) has been recognized as a promising non-invasive diagnostic tool for the early detection of ischemic heart disease, arrhythmia, and fetal diagnosis [5], [6].

It allows monitoring of magnetic field changes related to the spontaneous electrical activity of the heart from multiple locations above the chest [7]. Changes in cardiac electrical activation during depolarization and repolarization, which may be caused by ischemia and reversible coronary artery disease [8], are detected and quantified as changes in magnetic field distribution on the chest [9].

Compared to ECG, MCG provides additional information, and is more sensitive to tangential currents, and capable to detect vortex currents. Besides, the cardiac magnetic field

The associate editor coordinating the review of this manuscript and approving it for publication was Joewono Widjaja.

is less affected by tissue conductivities [10], [11]. In addition, MCG has higher reproducibility, less signal fluctuation, and better spatial resolution [8], [9], [12]. Therefore, the promising technology has motivated the interest of scientists.

However, there are some deficiencies in MCG. The magnetic fields of the heart are too weak to measure with a magnitude of 10^{-11} Tesla. So, most MCG systems currently operate in magnetic shielding chambers to detect very weak cardiac magnetic fields. Besides, it requires more specialized knowledge to make a diagnosis than an ECG does. One of the main reasons may be the absence of diagnostically clear criteria providing high sensitivity and specificity. Therefore, diagnosis technology based on computers is of great value to clinicians.

Machine learning is a promising data analysis technique. This technology can discover new knowledge from data sets, and can explore the unknown laws and trends from different data sets. Li *et al.* [13], Ren *et al.* [14], Yuan *et al.* [15], and Faramarzi *et al.* [16]. They have made good progress in machine learning methods.

Besides, this technique has widely been adopted for biomedical applications. Embrechts *et al.* [17] used direct kernel partial least squares(DK-LPS) to separate abnormal heart beats from normal ones, with accuracy of 83%. Fan *et al.* [18] used support vector machine(SVM) to analyse 12 morphological features from ECG ST segments, with accuracy of 95.2%. Udovychenko *et al.* [19] used k-nearest neighbor (K-NN) to binary classify current density distribution maps, with accuracy in a range of 80-88%, 70-95%. Tao *et al.* [20] used XGBoost classifier and 18 time domain features to detect IHD, with accuracy of 94.03%. Tantimongcolwat *et al.* [21] used BNN to classify MCG data of IHD, with accuracy of 74.5%. Steinisch *et al.* [22] classified Zorr50% of neural networks by using multi-layer perceptron (MLP) neural network based on Linear Discriminant analysis (LDA). The best results for MCG at rest were 98% accuracy for a single heartbeat. Huang *et al.* [23] used multilayer perceptron (MLP) neural network to investigate the usefulness of the MCG to detect CAD. The two models with accuracy 89.5% and 90.0%.

Past studies show promising results in the automatic detection of IHD. However, those studies require prior knowledge and are influenced by some subjective factors in feature selection. Compared with machine learning methods, the deep learning method such as ResNet requires less prior knowledge, and can mine the internal laws of data sets automatically through building the deep network, which can reduce the influence of human subjective factors.

Odusami *et al.* [24] used finetuned ResNet-18 network to detect early stage from functional brain changes in functional magnetic resonance images(fMRI), with accuracy of 99.9%. Al-Falluji [25] used modified ResNet-18 network and chest X-Ray images to automatically detect COVID-19, with accuracy of 96.73%.

II. METHODS

The framework of current density vector map (CDVM) classification as shown in Fig. 1.

A. DATASETS

The data was collected by "pulse pump Rb atomic magnetometer" [26], [27], which can collect MCG data from 49 channels. The collected multichannel MCG data are shown in Fig.2.

It is hard to classify IHD from raw data, so we reconstruct the CDVM from raw data, which can reflect the complex source structure associated with distributed excitation wavefronts within the heart [28]. The CDVM has made great progress in ischemic heart disease detection [19], [28].

The CDVMs can be classified from category 0 (normal) to category 4 (grossly abnormal). One example shows in Fig. 3, which is given for each of the 5 categories.

As a clinical diagnostic method, CDVMs have two parameters to diagnose whether this person suffers from cardiac diseases [29]. One is average classification of total maps (ACTM), if ACTM $\geq$ 3.0 is abnormal, while ACTM $<$ 3.0 is normal. Let n denotes the number of samples, i denotes sample i, c_i denotes the category of sample i. ACTM can be formulated in Eq. (1).

$$\text{ACTM} = \frac{\sum_{i=1}^{n} c_i}{n} \tag{1}$$

Another parameter is the ratio of abnormal maps (RAM), which shows the proportion of abnormal CDVMs(category 3 and category 4) in all CDVMs. If RAM $\geq$ 50% is abnormal, while RAM $<$ 50% is normal. Let n denotes the number of samples, i denotes sample i. If sample i is category 3 or 4, $a_i = 1$, else 0. RAM can be formulated in Eq. (2), Eq. (3).

$$\text{RAM} = \frac{\sum_{i=1}^{n} a_i}{n} \tag{2}$$

$$a_i = \begin{cases} 1, & \text{sample } i \text{ is category 3 or 4,} \\ 0, & \text{else.} \end{cases} \tag{3}$$

After removing the samples with poor quality of MCG, a total of 23 experimental samples are left in this task, including 16 normal people and 7 patients. CDVM is reconstructed every 10 ms in the ST-T segment from the J point to the end of the T-wave, according to Fig. 4.

About 15 CDVMs need to be reconstructed from each sample based on the single cardiac magnetic periodic signal. One example of the generation of MCG raw data to CDVMs is shown in Fig. 5. Finally, a total of 341 CDVMS were reconstructed.

Not all of the CDVMs reconstructed from patients are category 3 or category 4, they can be category 0, category 1 or category 2. So, all original CDVMs need to be sent to experts for annotation and classification. There are 100 CDVMs of category 0, 107 CDVMs of category 1, 97 CDVMs of category 2, 96 CDVMs of category 3, 110 CDVMs of category 4. For each category, the data is divided into training set, validation set and test set in a 6:2:2 ratio.

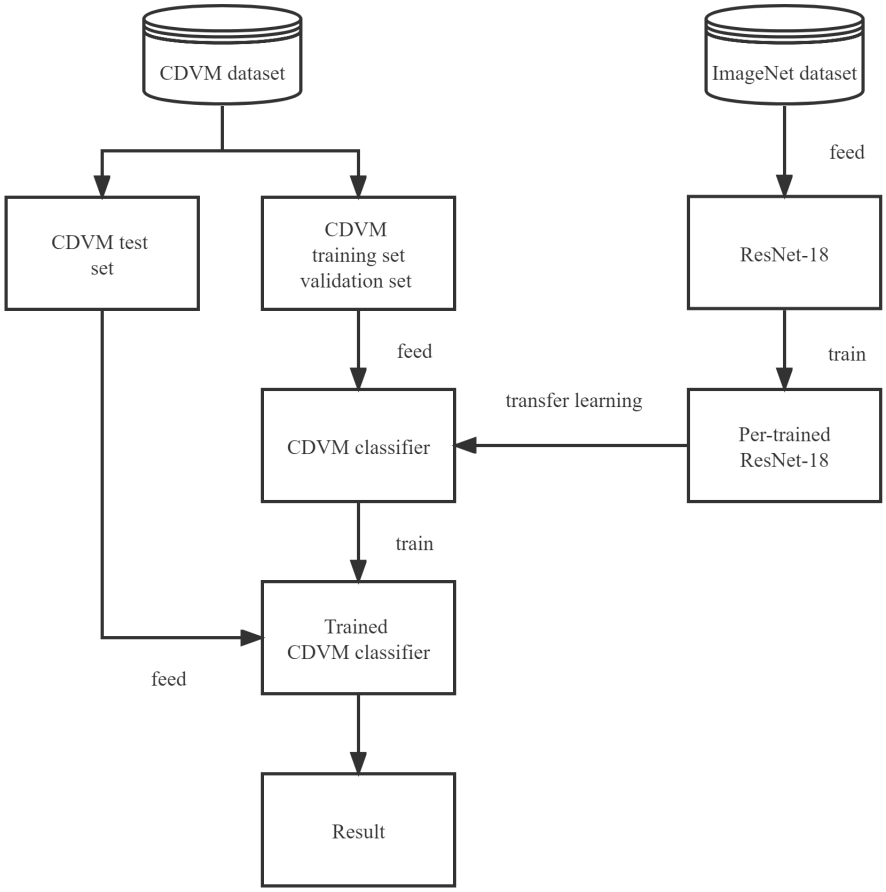

FIGURE 1. CDVM classification framework.

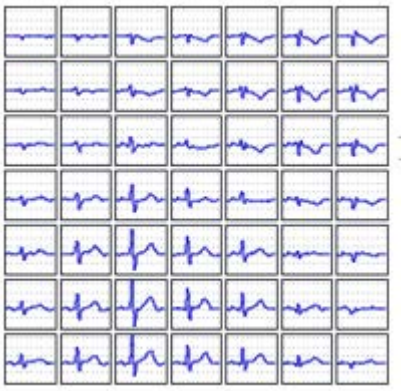

FIGURE 2. Multichannel MCG data.

Training a large neural network requires a large number of labeled data sets. It is obvious that the CDVMs in our hands are not enough to handle this classification task. In view of the current insufficient data sets, we use the method of manual enhancement to amplify the data set, which can add multiple copies to each original image. In this way, the overfitting of network can be reduced and the generalization ability of network model can be improved. Data enhancement mainly includes: contrast changing, brightness changing, chroma changing, image sharpening, random noise increasing. One example of data enhancement is shown in Fig.6.

After data enhancement, the enhanced images are mixed with the original data set. Then, a total of 1705 CDVMs are available for experiment. So we have 1023 CDVMs in the training set, 341 CDVMs in the validation set and 341 CDVMs in the test set. Therefore, datasets and labels are built in this task.

B. DEEP LEARNING

In this task, we need to train a five-classification classifier. We feed CDVMs to the classifier, then we will know which category it is. Here, deep learning method such as ResNet-18 is used as the five-classification classifier.

C. ResNet-18

ResNet means deep residual network, a type of Convolutional Neural Network (CNN) proposed by He *et al.* [30]. ResNet-18 is a type of ResNet, which has 17 convolutional layers (conv) and 1 fully connected layer (FC). Different with plain network, ResNet has shortcut connections to skip blocks of convolutional layers, which can effectively avoid vanishing and exploding gradients in deep CNN.

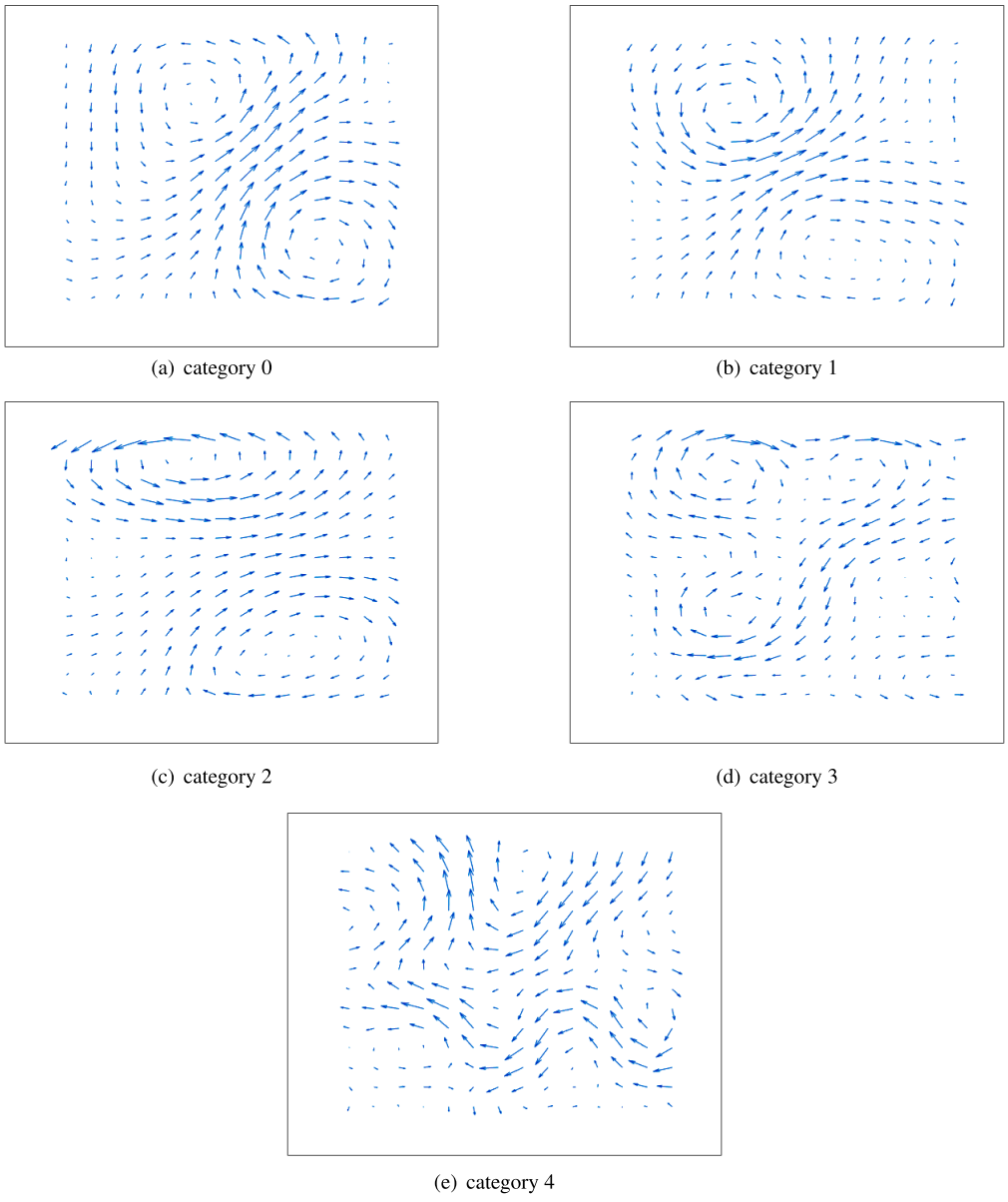

(a) category 0 (b) category 1

(c) category 2 (d) category 3

(e) category 4

FIGURE 3. Classification system of CDVM: one example is given for each of the 5 categories (0-4).

Several convs, batch normalizations (BN), Relu activation function and one short cut form a Residual BasicBlock (RB). There are two types of Rb in ResNet-18.

The RB-1 in ResNet-18 has 2 convs, BN, Relu and an identity x short cut, as shown in Fig. 7(a). Let y denotes the output, x denotes the input, F denotes the nonlinear function for the convolutional path in RB-1. The output of RB-1 can be formulated in Eq. (4). The x through the nonlinear function $F(x)$, and plus x becomes the output y of RB-1. The input x and output y are in the same dimensions.

The RB-2 in ResNet-18 has 2 convs, BN, Relu and a convolutional short cut, as shown in Fig. 7(b). Let y denotes the output, x denotes the input, F denotes the nonlinear function for the convolutional path in RB-2, H denotes the convolutional short cut. The output of RB2 can be formulated in Eq. (5). The x through the nonlinear function F, and plus x through convolutional short cut $H(x)$ becomes the output(y) of RB-2. The input x and output y are not in the same shape. Convolutional path is responsible for reducing output size and then increasing dimensions. Two types of resident block are shown in Fig.7.

$$y = F(x) + x \tag{4}$$

$$y = F(x) + H(x) \tag{5}$$

D. TRANSFER LEARNING

Usually, deep learning methods need a large amount of data to train a neural network. The large amount of data can help deep

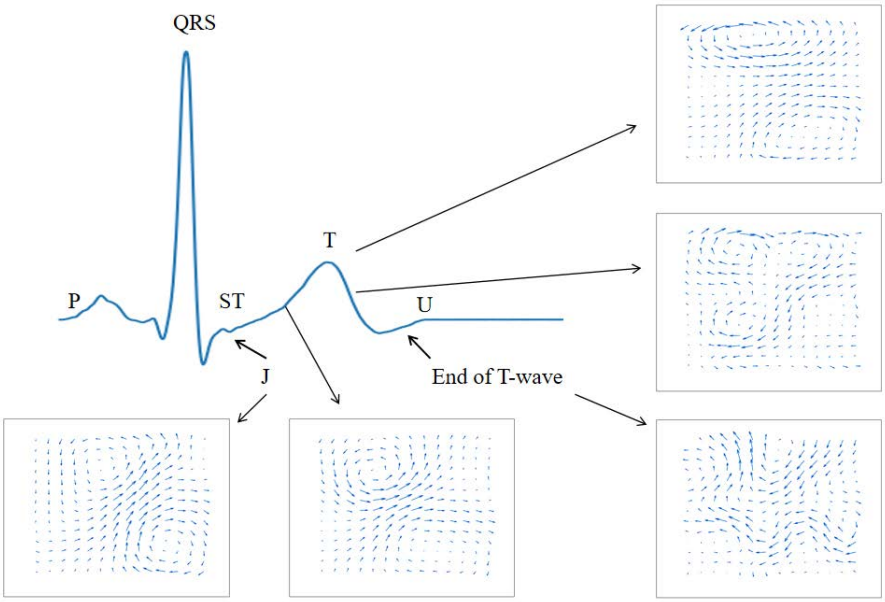

FIGURE 4. Reconstruction of CDVM from J point to the end of the T-wave.

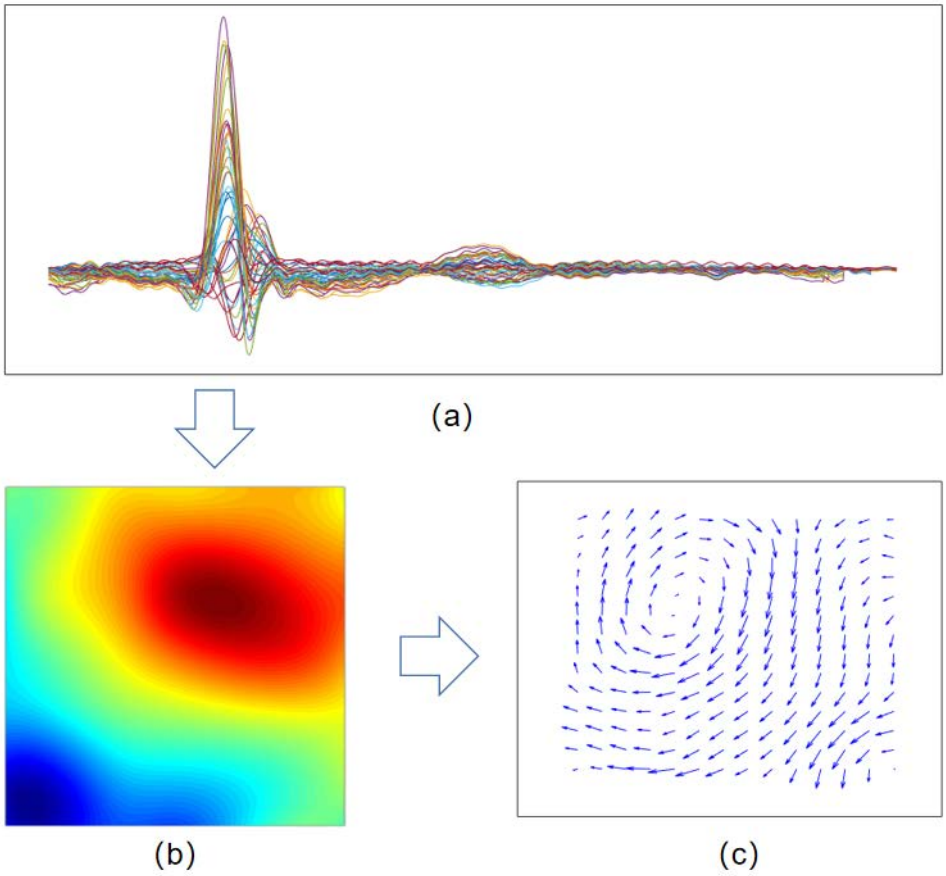

FIGURE 5. Generation of current density vector map: (a) An example of MCG signals in all channels. (b) Corresponding magnetic field map. (c) Corresponding current density vector map.

neural network to learn the features of CDVMs. But, it's hard to train a deep neural network for us because we don't have access to large amounts of well-organized data like ImageNet. Some researchers train deep CNN models on ImageNet [31],

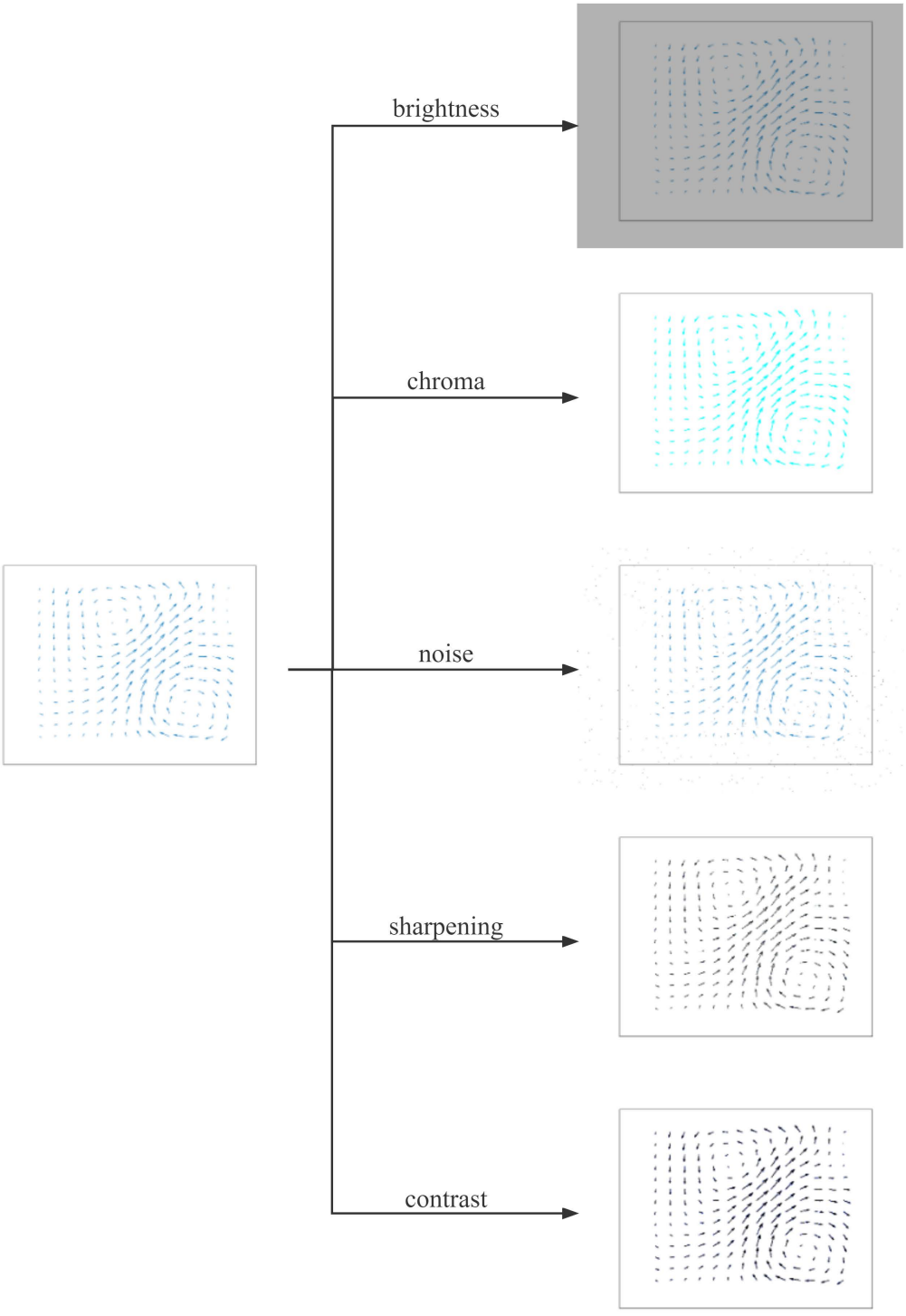

FIGURE 6. Examples of data enhancement include: contrast changing, brightness changing, chroma changing, image sharpening, random noise increasing.

and then apply trained CNN models as feature extractors in another field by transfer learning techniques [32], [33]. They have achieved good results.

Transfer learning is a technology that takes knowledge the neural network has learned from one task and applies that knowledge to another task. Schematic diagram of transfer learning are shown in Fig.8. How to pre-train a model is an important part. We will follow the following steps:

1) Find a proper model
   It's difficult to train a deep neural network from random initialization. Sometimes this training takes several

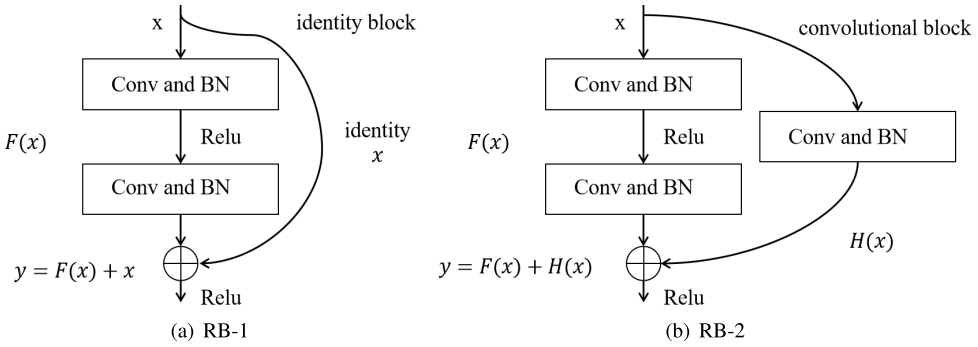

FIGURE 7. Two types of resident block.

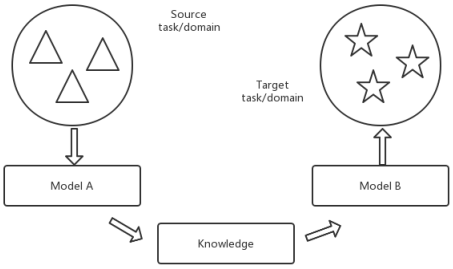

FIGURE 8. Schematic diagram of transfer learning.

weeks. But, there is someone else who has finished this training. We can download weights that some else has already trained and use that as per-training and transfer that to a new task.

2) Reuse the model
The model chosen in step one will be reused in the new task. Reuse the model includes part of the model or all of the model.

3) Fine tuning
After applying weights to initialize our own neural network, we can freeze parameters in some layers, transfer fully connected layer and then train in our own dataset. Usually, the neural network can be more accurate than we just train from random initialization.

E. TRANSFER LEARNING ON ResNet-18

The features have learned in ImageNet can be applied to CDVMs to classify. After applying parameters trained by others to our own ResNet, we transfer 1000-dimensions fc to 5-dimensions fc to fit the CDVM classification task. Then we freeze the first two RB layers as the bottom features extraction of image. Deep learning methods impersonate the functioning of the human brain in methodology information. The first few layers of the deep learning model identify simple features, the middle layers identify more complex features and patterns, and the last layer is used for prediction. So the first two RB layers of ResNet are similar as feature extraction at the bottom level of pictures. Finally, the structure of the proposed ResNet-18 is presented in Fig. 9.

Before the network training, the size of the images of the training set, validation set and test set should be set to 224 × 224. Then, the pre-processed images are fed into the network model for training. Finally, the network works well and then we save the network weights for subsequent identification and classification.

The training of neural network often requires a large amount of training data, but it is difficult to feed all the training data into the network at one time. We can feed the data set into the network model in batches. The volume of batches is called batch size. In the task, we set the batch size to 8.

After the input image forward propagation, the SoftMax classifier calculates the probability of each sample input for each category, and then calculates the loss value of the sample using the loss function. In this task, the Cross Entropy Loss function is used as the loss function of the network model. Let C denotes the output, n denotes the number of all samples, y denotes the true label, $\hat{y}$ denotes the prediction of samples. The equation of Cross Entropy Loss function is shown in Eq. (6).

$$C = -\frac{1}{n}\sum_{x}[yln\hat{y} + (1-y)ln(1-\hat{y})] \tag{6}$$

As we know, the purpose of neural network learning is to find appropriate parameters to make the value of the loss function as small as possible. So after calculating the loss, we need a tool to make it smaller. This tool is called optimizer. There are many kinds of optimizers for neural networks. Adaptive Moment Estimation (Adam) is adopted in this task, which combines Adaptive Gradient (AdaGrad) and Root Mean Square Propagation (Root Mean Square Propagation). The algorithm of Adam is shown in algorithm (1).

Learning rate is a very important hyperparameter in the process of network training, which controls the updating speed of the weight parameters of the network model and determines the convergence speed of the network model. If the learning rate is too small, it is easy to fall into the local optimal solution; otherwise, if the learning rate is too large, it is easy to miss the optimal solution. In this experiment, we set the learning rate of the network model as 0.0001.

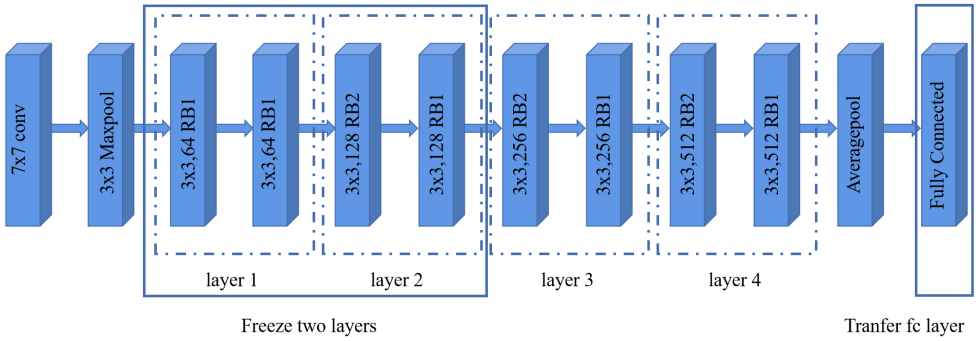

FIGURE 9. A view of ResNet-18 after fine tuning.

Algorithm 1 Adam

Require: α : Stepsize
Require: $\beta_1, \beta_2 \in [0, 1)$: Exponential decay rates for the moment estiamtes
Require: ϵ : A small constant used for numerical stability
Require: θ : Initialize parameter vector
$m_0 = 0$: Initialize first moment vector
$v_0 = 0$: Initialize second moment vector
$t = 0$: Initialize timestep
while θ_t not converged **do**
$t \leftarrow t + 1$;
$g_t \leftarrow \nabla_\theta f_t(\theta_{t-1})$; (Get gradients)
$m_t \leftarrow \beta_1 \cdot m_{t-1} + (1 - \beta_1) \cdot g_t$; (Update biased first moment estimate)
$v_t \leftarrow \beta_2 \cdot v_{t-1} + (1 - \beta_2) \cdot g_t$; (Update biased second moment estimate)
$\hat{m}_t \leftarrow \frac{m_t}{1-\beta_1^t}$; (Compute bias-corrected first moment estimate)
$\hat{v}_t \leftarrow \frac{v_t}{1-\beta_2^t}$; (Compute bias-corrected second moment estimate)
$\theta_{t+1} \leftarrow \theta_t - \alpha \cdot \frac{\hat{m}_t}{\sqrt{\hat{v}_t}+\epsilon}$; (Update parameters)
$\theta \leftarrow \theta + \bigtriangleup \theta$; (Update parameters)
end while

TABLE 1. Hyperparameters of ResNet-18.

loss function	Cross Entropy
optimizer	Adam
learning rate	0.0001
epoch	200
batch size	8

In a word, the hyperparameters for the proposed ResNet-18 used during training set, validation set and test set are shown in Table1.

III. RESULT

In this task, we choose confusion matrix to value the model. The confusion matrix is shown in Fig.10. From the confusion matrix, most of the input can be predicted well, but some samples of category 3 are likely to be predicted to be category 4, and little of the samples of category 0 are likely to be predicted to be category 1.

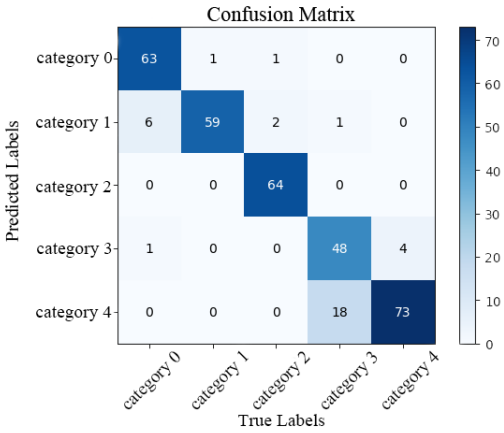

FIGURE 10. Confusion matrix of test set.

To evaluate classification result, the following parameters are used: precision, recall, specificity and accuracy. These values are defined as follows:

$$\text{Precision} = \frac{\text{TP}}{\text{TP} + \text{FP}} \tag{7}$$

$$\text{Recall} = \frac{\text{TP}}{\text{TP} + \text{FN}} \tag{8}$$

$$\text{Specificity} = \frac{\text{TN}}{\text{TN} + \text{FP}} \tag{9}$$

$$\text{Accuracy} = \frac{\text{TP} + \text{TN}}{\text{TP} + \text{FP} + \text{TN} + \text{FN}} \tag{10}$$

where TP(True positive): number of True samples predicted as positive, FP(False positive): number of False samples predicted as positive, FN(False negative): number of False samples predicted as negative, FP(False positive): number of False samples predicted as positive. The mean accuracy of ResNet is 90.02%. Precision, recall, specificity for each category are shown in Table.3.

The training accuracy of training set rapidly rises in the first 25 epochs, and then reaches about 90%, and the accuracy of validation set reaches about 88%. The ResNet performs good

TABLE 2. Precision, Recall, Specificity, Accuracy of ResNet-18 for each category.

	Precision	Recall	Specificity
category 0	96.9%	90.0%	99.3%
category 1	86.8%	98.3%	96.8%
category 2	100%	95.5%	100%
category 3	90.6%	71.6%	98.2%
category 4	80.2%	94.8%	93.2%

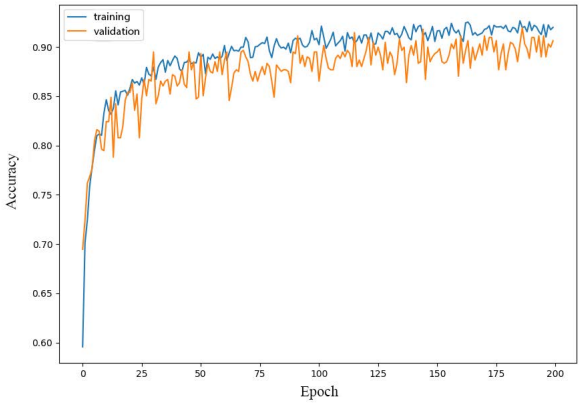

FIGURE 11. Training accuracy in each epoch.

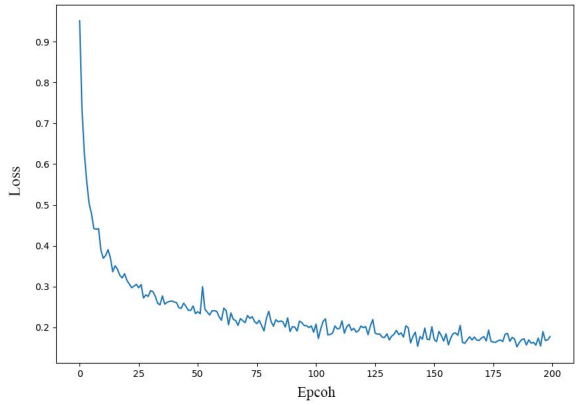

FIGURE 12. Training loss in each epoch.

in both training set and validation set. The training accuracy in each epoch is as shown in Fig.11.

The training loss rapidly declines in the first 100 epochs, and then reaches about 0.2. The training loss still has a trend to go down, which shows with the epoch bigger the ResNet works better. The training loss in each epoch is as shown in Fig.12.

Besides, we also train a support vector machines(SVM), with the same input of ResNet, to compare with ResNet. The accuracies of SVM with different kernels are shown in Table.3. Both of these three methods perform good in train set, while the accuracy of test set preform bad, which shows the superiority of ResNet in CDVM classification.

Compared with other non-invasive diagnosis of cardiac disease such as rest and stress ECG, MCG as a new technique performs very well. CDVMs reconstructed from MCG makes obvious images for doctors to diagnosis. And the result suggests a high potential of applying ResNet for CDVMs.

TABLE 3. Classification results of SVM with different kernel functions.

Kernel function	accuracy of train set	accuracy of test set
linear kernel	96.04%	70%
poly kernel	90.11%	74%
rbf kernel	96.04%	22%

IV. DISCUSSION

In this paper, we propose an automatic CDVM classification system based on transfer learning on ResNet-18. Compared with SVM, it requires less prior knowledge and the result shows the superiority of ResNet in CDVM classification. According to ACTM and RAM, our system is suitable for early detection of cardiac diseases. The mean accuracy of our system reaches 90.02%, but there are still some problems that need to be solved. The reasons for the accuracy just reaches 90.02% may be as follows: firstly, although transfer learning can help reduce the influence of small datasets, within limits, the more data we have, the better the network will perform. Secondly, we only have a small amount of patients' data, which mainly leads to confusing category 3 and 4. Thirdly, the ResNet-18 is used in this task. Only 18 layers in this ResNet, the deeper ResNet named ResNet-50 may be better in CDVM classification.

DISCLOSURES

The authors declare no conflicts of interest.

REFERENCES

[1] F. Sanchis-Gomar, C. Perez-Quilis, R. Leischik, and A. Lucia, "Epidemiology of coronary heart disease and acute coronary syndrome," *Ann. Transl. Med.*, vol. 4, no. 13, p. 256, Jul. 2016.
[2] M. Zhou, H. Wang, X. Zeng, P. Yin, J. Zhu, W. Chen, X. Li, L. Wang, L. Wang, Y. Liu, and J. Liu, "Mortality, morbidity, and risk factors in China and its provinces, 1990–2017: A systematic analysis for the global burden of disease study 2017," *The Lancet*, vol. 394, no. 10204, pp. 1145–1158, 2019.
[3] *World Health Report*, W. H. Organisation, Geneva, Switzerland, 2013.
[4] T. Tantimongcolwat, T. Naenna, C. Isarankura-Na-Ayudhya, M. J. Embrechts, and V. Prachayasittikul, "Identification of ischemic heart disease via machine learning analysis on magnetocardiograms," *Comput. Biol. Med.*, vol. 38, no. 7, pp. 817–825, Jul. 2008.
[5] E. A. P. Alday, H. Ni, C. Zhang, M. A. Colman, Z. Gan, and H. Zhang, "Comparison of electric- and magnetic-cardiograms produced by myocardial ischemia in models of the human ventricle and torso," *PLoS ONE*, vol. 11, no. 8, Aug. 2016, Art. no. e0160999.
[6] I. Tavarozzi, S. Comani, C. Del Gratta, G. L. Romani, S. Di Luzio, D. Brisinda, S. Gallina, M. Zimarino, R. Fenici, and R. De Caterina, "Magnetocardiography: Current status and perspectives. part i: Physical principles and instrumentation," *Ital Heart J*, vol. 3, no. 2, pp. 75–85, 2002.
[7] K. Tsukada, D. Eng, H. Sasabuchi, and T. Mitsui, "Measuring technology for cardiac magneto-field using ultra-sensitive magnetic sensor—For high speed and noninvasive cardiac examination," Tech. Rep., 1999.
[8] S. Williamson, "Biomagnetism. Sources and their detection," *J Magnetism Magn Mater.*, vol. 22, 1981.
[9] H. Koch, "SQUID magnetocardiography: Status and perspectives," *IEEE Trans. Appl. Supercond.*, vol. 11, no. 1, pp. 49–59, Mar. 2001.
[10] K. Brockmeier, L. Schmitz, J. D. J. B. Chavez, M. Burghoff, and L. Trahms, "Magnetocardiography and 32-lead potential mapping: Repolarization in normal subjects during pharmacologically induced stress," *J. Cardiovascular Electrophysiol.*, vol. 8, no. 6, pp. 615–626, 2010.

[11] R. Fenici, D. Brisinda, and A. M. Meloni, "Clinical application of magnetocardiography," *Expert Rev. Mol. Diag.*, vol. 5, no. 3, pp. 291–313, May 2005.
[12] S. Yamada and I. Yamaguchi, "Magnetocardiograms in clinical medicine: Unique information on cardiac ischemia, arrhythmias, and fetal diagnosis," *Internal Med.*, vol. 44, no. 1, pp. 1–19, 2005.
[13] S. Li, H. Chen, M. Wang, A. A. Heidari, and S. Mirjalili, "Slime mould algorithm: A new method for stochastic optimization," *Future Gener. Comput. Syst.*, vol. 111, pp. 300–323, Oct. 2020.
[14] J. Ren, Z. Wang, Y. Pang, and Y. Yuan, "Genetic algorithm-assisted an improved AdaBoost double-layer for oil temperature prediction of TBM," *Adv. Eng. Informat.*, vol. 52, Apr. 2022, Art. no. 101563.
[15] Y. Yuan, X. Mu, X. Shao, J. Ren, Y. Zhao, and Z. Wang, "Optimization of an auto drum fashioned brake using the elite opposition-based learning and chaotic k-best gravitational search strategy based grey wolf optimizer algorithm," *Appl. Soft Comput.*, vol. 123, Jul. 2022, Art. no. 108947.
[16] A. Faramarzi, M. Heidarinejad, B. Stephens, and S. Mirjalili, "Equilibrium optimizer: A novel optimization algorithm," *Knowl.-Based Syst.*, vol. 191, Mar. 2020, Art. no. 105190.
[17] M. Embrechts, B. Szymanski, K. Sternickel, T. Naenna, and R. Bragaspathi, "Use of machine learning for classification of magnetocardiograms," in *Proc. IEEE Int. Conf. Syst., Man Cybernetics. Conf. Theme Syst. Secur. Assurance (SMC)*, Oct. 2003, pp. 1400–1405.
[18] C.-H. Fan, Y. Hsu, S.-N. Yu, and J.-W. Lin, "Detection of myocardial ischemia episode using morphological features," in *Proc. 35th Annu. Int. Conf. IEEE Eng. Med. Biol. Soc. (EMBC)*, Jul. 2013, pp. 7334–7337.
[19] Y. Udovychenko, A. Popov, and I. Chaikovsky, "K-NN binary classification of heart failures using myocardial current density distribution maps," in *Proc. Signal Process. Symp. (SPSympo)*, Jun. 2015.
[20] R. Tao, S. Zhang, X. Huang, M. Tao, J. Ma, S. Ma, C. Zhang, T. Zhang, F. Tang, J. Lu, C. Shen, and X. Xie, "Magnetocardiography-based ischemic heart disease detection and localization using machine learning methods," *IEEE Trans. Biomed. Eng.*, vol. 66, no. 6, pp. 1658–1667, Jun. 2019.
[21] T. Tantimongcolwat, T. Naenna, C. Isarankura-Na-Ayudhya, M. J. Embrechts, and V. Prachayasittikul, "Identification of ischemic heart disease via machine learning analysis on magnetocardiograms," *Comput. Biol. Med.*, vol. 38, no. 7, pp. 817–825, Jul. 2008.
[22] M. Steinisch, P. R. Torke, J. Haueisen, B. Hailer, D. Grönemeyer, P. Van Leeuwen, and S. Comani, "Early detection of coronary artery disease in patients studied with magnetocardiography: An automatic classification system based on signal entropy," *Comput. Biol. Med.*, vol. 43, no. 2, pp. 144–153, Feb. 2013.
[23] X. Huang, P. Chen, F. Tang, and N. Hua, "Detection of coronary artery disease in patients with chest pain: A machine learning model based on magnetocardiography parameters," *Clin. Hemorheol. Microcirculation*, vol. 78, no. 3, pp. 1–10, 2020.
[24] M. Odusami, R. Maskeliūnas, R. Damaševičius, and T. Krilavičius, "Analysis of features of Alzheimer's disease: Detection of early stage from functional brain changes in magnetic resonance images using a finetuned ResNet18 network," *Diagnostics*, vol. 11, no. 6, p. 1071, Jun. 2021.
[25] R. A. Al-Falluji, Z. D. Katheeth, and B. Alathari, "Automatic detection of COVID-19 using chest X-ray images and modified ResNet18-based convolution neural networks," *Comput., Mater. Continua*, vol. 66, no. 2, pp. 1301–1313, 2021.
[26] M. Bai, Y. Huang, G. Zhang, W. Zheng, Q. Lin, and Z. Hu, "Fast backward singular value decomposition (SVD) algorithm for magnetocardiographic signal reconstruction from pulsed atomic magnetometer data," *Opt. Exp.*, vol. 27, no. 21, pp. 29534–29546, 2019.
[27] H. E. Xiang, Y. Huang, L. I. Shuguang, S. U. Shengran, W. Zheng, H. U. Zhenghui, and Q. Lin, "Measurement of cardiac magnetic field based on atomic magnetometry," *Chin. J. Med. Phys.*, 2017.
[28] B. Hailer, I. Chaikovsky, S. Auth-Eisernitz, H. Schafer, and P. Van Leeuwen, "The value of magnetocardiography in patients with and without relevant stenoses of the coronary arteries using an unshielded system," *Pacing Clin. Electrophysiol.*, vol. 28, no. 1, pp. 8–16, Jan. 2005.
[29] W.-W. Quan, G.-P. Lu, W.-H. Qi, Y.-M. Li, Y. Shen, and R. Yuan, "Diagnostic value of magnetocardiography in patients with coronary heart disease and in-stent restenosis," *Chin. Med. J.*, vol. 121, pp. 6–22, Jan. 2008.
[30] K. He, X. Zhang, S. Ren, and J. Sun, "Deep residual learning for image recognition," in *Proc. IEEE Conf. Comput. Vis. Pattern Recognit. (CVPR)*, Jun. 2016, pp. 770–778.
[31] A. Krizhevsky, I. Sutskever, and G. E. Hinton, "ImageNet classification with deep convolutional neural networks," *Commun. ACM*, vol. 60, no. 6, pp. 84–90, May 2017.
[32] J. Donahue, Y. Jia, O. Vinyals, J. Hoffman, N. Zhang, E. Tzeng, and T. J. Darrell, "DECAF: A deep convolutional activation feature for generic visual recognition," Tech. Rep., 2014.
[33] J. Yosinski, J. Clune, Y. Bengio, and H. Lipson, "How transferable are features in deep neural networks?" in *Proc. Adv. Neural Inf. Process. Syst.*, vol. 27, 2014, pp. 1–9.

ZHENGHUI HU received the Ph.D. degree in physics from Zhejiang University, Hangzhou, China, in 2005. From 2005 to 2007, he was a Postdoctoral Fellow in electrical and computer engineering with The Hong Kong University of Science and Technology. From 2008 to 2010, he was a Postdoctoral Fellow in computing and information science with the Rochester Institute of Technology, Rochester, NY, USA. Since 2015, he has been a Professor with the College of Science, Zhejiang University of Technology, Hangzhou. His research interests include functional brain imaging, magnetocardiography, and signal reconstruction.

YUTONG LIN is currently pursuing the master's degree with the College of Science, Zhejiang University of Technology. His research interests include deep learning methods and magnetocardiography classification.

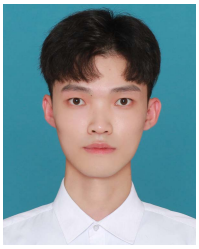

KAIKAI YE received the master's degree from the College of Science, Zhejiang University of Technology. His research interests include MCG signal processing and magnetocardiography classification.

QIANG LIN was born in Zhejiang, China, in July 1964. He received the M.S. degree in optics from Hangzhou University, in 1988, and the Ph.D. degree from Zhejiang University, in 2003. He was a Professor and the Head of the Optics Division, Department of Physics, Hangzhou University, in 1994. From 1996 to 1997, he was with the Technical University of Vienna, Austria. In 1998, he joined the Department of Physics, Zhejiang University, and became the Director of the Optics Institute. From 2005 to 2006, he was an Alexander von Humboldt Fellow with the Max-Born-Institute, Berlin, Germany. Since 2014, he has been the Dean of the College of Science, Zhejiang University of Technology. He is the author or the coauthor of more than 200 scientific articles and three books.